Thickness-Induced Phase Evolution and Mechanical and Tribological Performance of Arc-Sprayed FeCrAl Coatings

Bauyrzhan Rakhadilov , Aidar Kengesbekov * , Umar Ibtasam , Nurtoleu Magazov , Elvira Akhmetova , Suresh Alapati *

Posted Date: 3 February 2026

doi: 10.20944/preprints202602.0084.v1

Keywords: FeCrAl Coatings; Arc Spraying; Surface Roughness; XRD Analysis; Phase Composition; Oxidation Behavior; Tribological Behavior

Article

Thickness-Induced Phase Evolution and Mechanical and Tribological Performance of Arc-Sprayed FeCrAl Coatings

Bauyrzhan Rakhadilov [1], Aidar Kengesbekov [2,*], Umar Ibtasam [2], Magazov Nurtoleu [2], Elvira Akhmetova [2] and Suresh Alapati [3,*]

[1] PlasmaScience LLP, Ust-Kamenogorsk, Kazakhstan.

[2] Institute of composite materials, Ust-Kamenogorsk, Kazakhstan.

[3] Department of Mechatronics Engineering, Kyungsung University, Busan, Korea.

* Correspondence: aidar.94.01@mail.ru (A.K.); suresh@ks.ac.kr (S.A.)

Abstract

In this study, we examined the influence of coating thickness on surface roughness, hardness, phase composition, and tribological behavior of arc-sprayed FeCrAl coatings deposited on steel substrates. We measured coating thickness, phase composition, and surface roughness using optical microscopy, X-ray diffraction (XRD), and profilometry, respectively. Results showed that surface roughness decreased with increasing coating thickness due to improved splat coalescence. However, Rockwell hardness remained nearly constant (at approximately 95 HRB), denoting a limited dependency on coating thickness. Using pin-on-disk tribometry, we found that the thickest coating showed the highest coefficient of friction (CoF, mean value of 0.864). This is because there is an increased tendency for the formation of hard oxide phases (Cr_2O_3 and Al_2O_3) in thicker coatings. These oxides increased friction by generating abrasive debris during sliding. The novelty of this work is that CoF is sensitive not only to surface morphology but also to thickness-dependent phase composition, whereas most previous studies found that CoF was primarily correlated with surface roughness only. Our research findings show that both microstructural and phase composition behavior during deposition are crucial for optimizing the friction and wear properties of FeCrAl coatings in high-temperature, steam-rich applications. Therefore, accurate control of oxidation behavior as a function of coating thickness can lead to more durable, reliable coatings in those environments.

Keywords: FeCrAl Coatings; Arc Spraying; Surface Roughness; XRD Analysis; Phase Composition; Oxidation Behavior; Tribological Behavior

1. Introduction

The demand for high-performance surface coatings has continued to increase in industrial applications experiencing harsh thermal, corrosive, or mechanical conditions. One alloy system that has gained global interest in recent years is the Iron-Chromium-Aluminum (FeCrAl) alloy. The combination of chromium with aluminum in a ferrous matrix offers excellent high-temperature oxidation and corrosion resistance, as well as acceptable mechanical stability. Such properties make FeCrAl coatings highly promising candidates for protective coating applications in thermally and chemically aggressive environments. At elevated temperatures, FeCrAl alloys develop a dense and adherent aluminum oxide (Al_2O_3/alumina) layer [1] through selective oxidation of aluminum. This scale grows under parabolic oxidation kinetics (the rate of oxidation decreases over time as the oxide layer thickens), which inhibits further diffusion. This acts as a protective barrier against further oxidation and degradation [2]. This protective alumina scale provides a high melting point and long-term thermal stability, even under cyclical thermal conditions. Further, the chromium promotes adhesion, enhances the stability of alumina scale, and maintains oxidation resistance even in humid

 doi:10.20944/preprints202602.0084.v1

or steam-rich environments [3]. Compared to traditional coatings such as chromium plating and nickel-chromium-based alloy coatings (which face environmental and regulatory concerns), FeCrAl offers a more environmentally friendly alternative with comparable or superior durability and performance. Previous studies have primarily focused on HVOF [4] and plasma-sprayed FeCrAl [5,6] and NiCoCrAlY [7] coatings. Although these coatings are effective, they are expensive and less scalable than arc spraying methods. To address this gap, the present study explores the performance of arc-sprayed FeCrAl coatings deposited on steel substrates under controlled laboratory conditions. Arc spraying is a thermal spraying technique that is both effective and cost-efficient for depositing metallic and alloy coatings. It works by melting two wires with an electric arc, then propelling molten droplets onto a substrate using a compressed gas stream [8,9]. This method is favored for its high deposition rates, ease of operation, and utility in large-scale processes. However, the quality and durability of the deposited coating are strongly influenced by process parameters, including arc current, spray distance, wire feed rate, substrate surface preparation [10], and post-treatment procedures [11–14]. Poor control over these parameters leads to microstructural defects, including porosity, poor adhesion, and uneven thickness distribution. The microstructural and mechanical properties of thermally sprayed coatings play a crucial role in determining their functionality and durability [9]. Key characteristics, such as coating thickness, surface roughness, hardness, and wear resistance, must be optimized to ensure that the coating withstands design loads, resists environmental degradation, and maintains structural integrity during prolonged service. For example, coating thickness directly affects mechanical strength, thermal insulation, and diffusion resistance. Surface roughness influences both adhesion and tribological behavior, whereas hardness and wear resistance are mainly affected by coating density and phase evolution during spraying. Early studies established fundamental relationships between spraying parameters and coating structure. Liu et al. [10] and Sarikaya [16] demonstrated that increasing substrate temperature and spray distance increases microhardness of iron-based coatings. They also found that when coating thickness increased, hardness showed limited variation while surface morphology evolved. Ataiwi [17] correlated wire feed rate, spraying distance, and voltage parameters with the wear resistance. They identified optimal parameter ranges that maximize coating density and microhardness. Later studies further emphasized that the wear and corrosion resistance of coatings were predominantly governed by microstructure distribution [18] and by the formation of an Al_2O_3 oxide layer [19], which acts as a protective layer on Zr-alloy tubes. Luo et al. [20] showed that increasing spraying power increases coating density but reduces the amorphous phase, thereby affecting both adhesion and wear resistance.

Based on the above findings, many researchers have recently shifted their focus to pre- and post-processing treatments. Li et al. [21] demonstrated that substrate surface preparation significantly affects density and surface uniformity. They proposed a composite polishing technique (combining electrolytic polishing and argon-ion-beam polishing) that correctly reveals the porosity of pure Al coatings. Li et al. [22] showed that post-treatment of FeCrAl coatings increases the coating density and improves the hardness. They also demonstrated that post-processed FeCrAl coatings exhibit improved oxidation resistance. Above literature study confirms that optimizing arc current, spraying distance, and wire feed rate enhances coating adhesion, increases density and oxidation stability, and pre- and post-treatment significantly affects the porosity.

Some researchers have also investigated oxide layer formation and its impact on corrosion resistance. Brundle et al. [23] and Yamashita and Hayes [24] investigated the chemical states of iron oxides using XPS and surface science techniques, which are relevant to the oxidation mechanism during FeCrAl thermal spraying. Cheng et al. [11] and Liu et al. [12] demonstrated that film chromaticity and oxide morphology significantly influence corrosion protection in stainless and carbon steels. Yuan et al. [2] and Liu et al. [15] examined oxidation in oxygen- and steam-rich environments, providing insight into the oxidation kinetics of Fe-based materials under high-temperature spray conditions. Similarly, Hu et al. [25] highlighted how oxide-dispersion-strengthened steels degrade in supercritical water (due to microstructural changes at high

 doi:10.20944/preprints202602.0084.v1

temperatures). This work suggests analogous phenomena may occur during our arc spraying. The heteroepitaxial growth of complex iron oxide films reported by Gao et al. [26] further supports the diversity of phases formed under non-equilibrium conditions. Comparative studies of new coating systems, i.e., TiN and oxide-based coatings, have also provided additional insights into the influence of some parameters on coating structure and functionality. For example, Kengesbekov et al. [27] and Pogrebnjak et al. [28] emphasized how arc current and elemental additions influence phase formation and tribological behavior. Mamaeva et al. [29] demonstrated how variations in voltage and duty cycle during plasma oxidation directly affect the microstructure of surface coatings. Similarly, Yermakhanova et al. [30] reported that processing conditions play a critical role in controlling dielectric properties and composite layer formation. These findings, though involving different materials, highlight the universal role of optimizing spray parameters in FeCrAl systems to achieve the required structural and functional properties. Collectively, these studies provide a strong scientific foundation for the present research. They demonstrate that, despite differences in material composition, the principles of oxidation kinetics, surface microstructure, and coating-process optimization apply universally to advanced surface engineering, such as FeCrAl coating systems for high-temperature and wear-intensive applications.

Despite a large number of parametric studies on FeCrAl coatings, few systematically examine the influence of thickness-induced oxidation kinetics alone on the mechanical and tribological performance of arc-sprayed FeCrAl coatings on steel. In the present study, this gap is addressed by examining the effect of coating thickness variation on surface roughness, hardness, and coefficient of friction, while all spraying parameters are kept constant. The present results provide practical insight into tailoring coating thickness to improve mechanical and tribological performance. These findings are relevant to the development of durable FeCrAl coatings for applications requiring wear and corrosion resistance.

2. Materials and Methods

2.1. Coating Preparation

The coating was arc-sprayed onto a low-carbon steel substrate using two consumable metal wires composed of FeCrAl alloy. Previous studies found that excessively high arc currents led to severe spattering and the formation of oxide layers, whereas the shorter stand-off distance resulted in localized melting and a non-uniform coating structure [8,31]. So, the experimental parameters in this study were optimized by considering parameter ranges reported in the literature [31], empirical relations, and preliminary experiments. The final process parameters selected for the present study were: arc current, 150 A; spray distance, 150 mm; and wire feed rate, 8 m/min. This optimized parameter set ensured a stable arc reaction, a smoothly flowing melt, and a uniform coating deposition.

We used the standard metallographic surface polishing procedure to prepare the coated samples for microstructural examination. Initially, the samples were cold-mounted in an epoxy resin. After that, the samples were ground and polished with a semi-automatic polishing machine under a controlled force and rotational speed. The final polishing step was performed using a MIRKA 5424105018 abrasive pad (Mirka Ltd., Finland). An oxide polishing suspension (OPS) with colloidal silica was applied during the final step. This procedure produces flat scratch-free surfaces suitable for high-resolution microscopy. This surface preparation was essential to achieve accurate observation of surface topography under a microscope, coating-substrate interface, and cross-sectional homogeneity.

2.2. Microstructural Characterization

We measured the thickness with cross-sectional optical microscopy. To ensure statistical significance, the thickness measurements were performed at three different locations of each specimen using 20X magnification, and four samples were considered. This method is widely used

 doi:10.20944/preprints202602.0084.v1

in thermal spray coating characterization and provides consistent and reproducible results. After measuring the thickness of the samples, we used a set of characterization techniques (XRD analysis, surface profilometry, Rockwell hardness test, pin-on-disk tribometry) to assess the structural, mechanical, and tribological properties of the FeCrAl coatings as shown in Figure 1. This approach enabled analysis of cause-and-effect relationships between process parameters, microstructure, and functional performance.

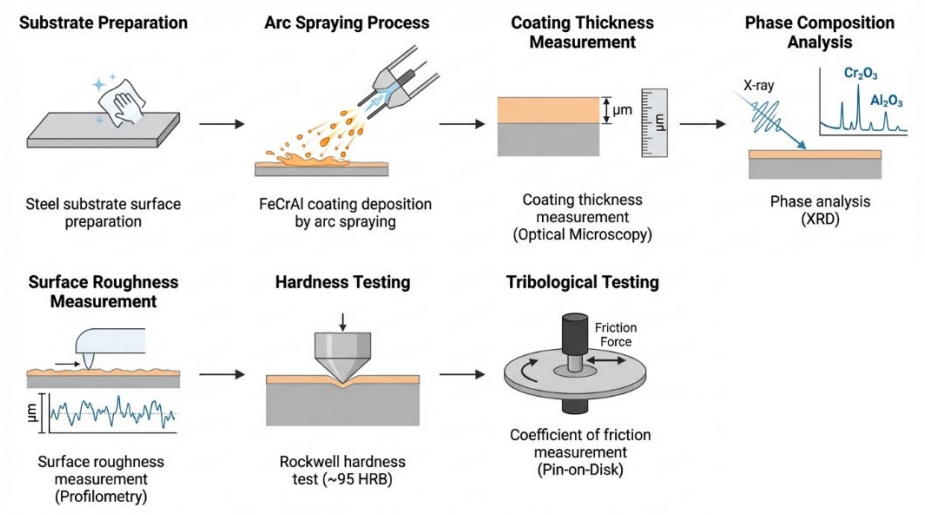

Figure 1. Schematic illustration of the experimental workflow for FeCrAl arc-sprayed coating preparation and characterization.

X-ray diffraction (XRD) analysis was carried out over an appropriate 2θ range to identify the crystalline phases. High temperatures and rapid solidification environment of the arc spraying process resulted in the formation of α-Fe matrix phase along with Cr-rich solid solutions and aluminum oxide (Al_2O_3) compounds. The presence of these oxides indicates partial in-flight oxidation of molten particles, which is a common phenomenon in arc-sprayed coatings that assists the thermal and oxidation resistance. The nature and distribution of these phases play a crucial role in governing the wear resistance and high-temperature durability of the coatings.

We measured the surface roughness of the coatings using a contact-type profilometer (iSurfa-310) across the standardized scan lengths. Key roughness parameters such as Ra, Rq, Rz, and Rt were extracted to evaluate the coating's topography. Higher Ra and Rz values are associated with splat boundaries and partially unmelted particle zones, whereas smoother regions generally correspond to higher hardness and better adhesion. These surface features strongly influence the tribological behavior and functional durability of coatings in industrial applications.

The mechanical strength of the coatings is characterized by Rockwell hardness measurements (HRB scale), which were performed in accordance with ASTM E18. We made five indentations at randomly selected locations on each sample and found the average hardness value. The measured hardness data reflected the combined effects of microstructural features, oxide dispersion, and density of coating. We observed a limited variation in hardness across samples. This indicates our coatings were prepared at consistent deposition conditions and good process repeatability.

The tribological behavior of the coatings was evaluated using a TRB3 pin-on-disk tribometer under dry sliding conditions. We conducted those tests with a normal load of 4.00 N, a sliding speed of 6.00 cm/s, and a wear track radius of 3.00 mm. The CoF value was continuously recorded and averaged over the steady-state sliding region. After conducting the tribological tests, we examined the wear tracks using optical microscopy to analyze wear mechanisms such as abrasive grooves, oxide layer delamination, and plastic deformation. We observed lower CoF values for denser coatings with reduced surface asperities.

 doi:10.20944/preprints202602.0084.v1

Statistical analyses were performed to assess the reliability and consistency of our measured properties. Standard deviation (SD) and coefficient of variation (CV) were calculated for coating thickness, surface roughness, and hardness data. In most cases, CV values remained below 5%, which confirms the precision and reproducibility of both the experimental techniques and the coating process. The following section presents the experimental findings and discusses their implication for arc-sprayed FeCrAl coatings.

3. Results & Discussion

3.1. Coating Thickness

We found that the cross-sectional thickness of the arc-sprayed FeCrAl coatings showed a measurable variation across all four samples. The recorded values were 215.95 µm, 226.08 µm, 266.47 µm, and 270.35 µm for samples 1 through 4, respectively (Figure 2). The difference between the thinnest and thickest coatings was 54.39 µm, corresponding to a variation of approximately 25%. The average thickness was 244.71 µm, with a SD of 24.14 µm, and a CV of 9.86%. This indicates coating thickness has moderate variability, which may influence coating mechanical and tribological performance.

As many parameters, such as spray current, standoff distance, wire feed rate, and torch path stability, influence the arc-spraying process, it is common to have such variability in coating thickness. Small deviations in torch angle or inconsistent manual operation can affect splat stacking efficiency and cause micro-level fluctuations in thickness. Variations in surface preparation, such as non-uniform sandblasting or differences in substrate roughness, can also impact droplet spreading and solidification behavior.

Although these thickness variations are within an acceptable range for arc-sprayed coatings, they can still affect mechanical and tribological properties, particularly in high-stress applications. Minor variation in thickness also influences oxide formation and phase evolution. Thinner regions may be more prone to early wear or delamination, whereas thicker ones can accumulate residual stresses or porosity. Below, we present the results of the effect of thickness on hardness, surface roughness, phase composition, and CoF.

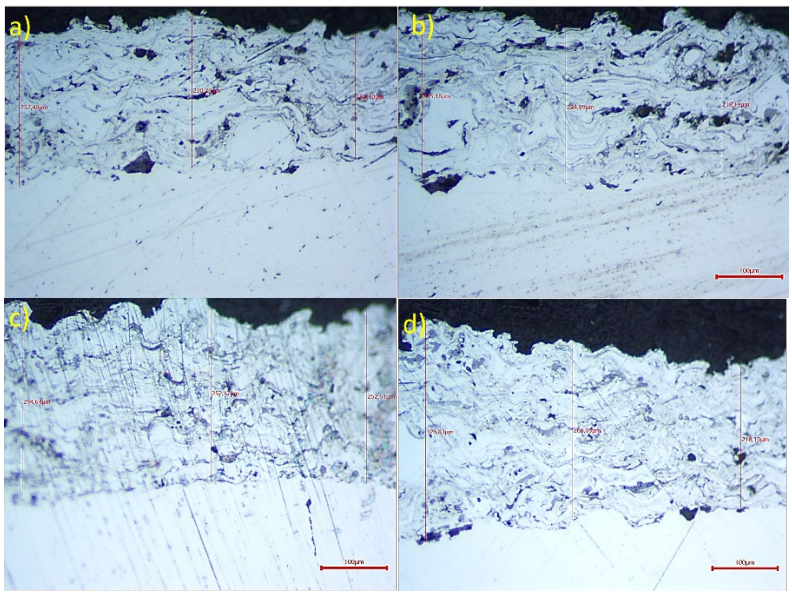

Figure 2. Cross-sectional thickness measurements of arc-sprayed FeCrAl coatings obtained by optical microscopy at 20X magnification.

3.2. Hardness

 doi:10.20944/preprints202602.0084.v1

The Rockwell hardness test showed that all four samples exhibited hardness values close to 95 HRB, with a SD of ±0.65 and a CV below 1% (Figure 3). This very low variation in the HRB values reflects a high level of mechanical uniformity, even though we observe a measurable variation in coating thickness (Section 3.1).

As expected for FeCrAl alloys, no clear relationship was found between coating thickness and hardness. Similar behavior was observed for FeCrAl coatings produced using thermal spray techniques [21]. In these coatings, hardness was found to be influenced by chromium and aluminum content, oxide dispersion, and rapid solidification during spraying, rather than by coating thickness. The consistent hardness values of our coatings also suggest low porosity and uniform splat bonding across all samples, indicating the formation of stable oxide phases (which agrees with the XRD analysis results discussed in Section 3.4).

Maintaining uniform hardness is essential for coatings exposed to mechanical wear or thermal cycling. The ability of the FeCrAl coatings in this study to retain their mechanical strength across different thicknesses provides flexibility for applications requiring variable coating thickness, such as turbine blades, heat exchangers, and automotive exhaust manifolds.

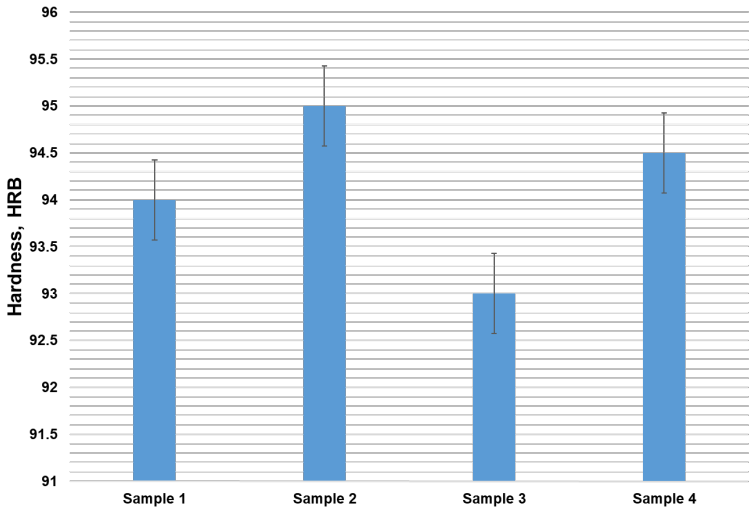

Figure 3. Rockwell hardness (HRB) of FeCrAl coating samples.

3.3. Surface Roughness

Surface roughness was characterized using the parameters Ra (average roughness), Rq (root mean square roughness), Rz (maximum peak-to-valley height), and Rt (total roughness height). Figure 4 shows all the sample parameter values that are also listed in Table 1. We found an inverse relationship between coating thickness and surface roughness. Thicker coating samples (Samples 3 and 4) had lower roughness values. Whereas Sample 1, with the lowest coating thickness, showed the highest roughness values. For Sample 1, Ra and Rz values of 24.89 μm and 162.09 μm were observed, respectively. This trend agrees well with previous studies on arc-sprayed FeCrAl coatings [10].

Table 1. Surface roughness parameters of all samples.

Samples	Ra (μm)	Rq (μm)	Rz (μm)
1	24.89	31.15	195.23
2	27.22	33.79	179.85
3	23.90	29.67	146.66
4	22.98	28.35	130.45

The decrease in the surface roughness with increasing coating thickness can be due to improved particle melting dynamics and splat coalescence. Thicker coatings generally promote the formation

 doi:10.20944/preprints202602.0084.v1

of more compact lamellar stacking that smooths the coating's surface. Increased deposition rates and high particle kinetic energy allow molten droplets to spread more uniformly when they impact. Molten droplets spread uniformly, covering substrate irregularities and filling microvoids, which reduces surface roughness and enhances integrity.

However, we observed an exceptional case in Sample 2 with the highest roughness values of Ra = 27.22 µm and Rz = 179.86 µm despite a relatively thicker coating. This might be due to factors other than coating thickness (e.g., variations in spray distance, wire feed rate, or surface preparation) that influenced the deposition process. In this sample, uneven splat coalescence or incomplete particle melting may also contribute to localized defects and increased surface roughness. To ensure the reliability of surface roughness measurements, we also conducted profilometer scans (three scans per sample) and found that the average SD of Ra was ±1.12 µm and the CV was approximately 4.7%. This demonstrates good measurement repeatability.

Smoother coatings are highly beneficial for critical applications such as sealing surfaces and thermal barrier layers, as they reduce friction and wear and improve dimensional accuracy. These results highlight that both coating thickness and stable spraying conditions are important factors in achieving consistent surface quality.

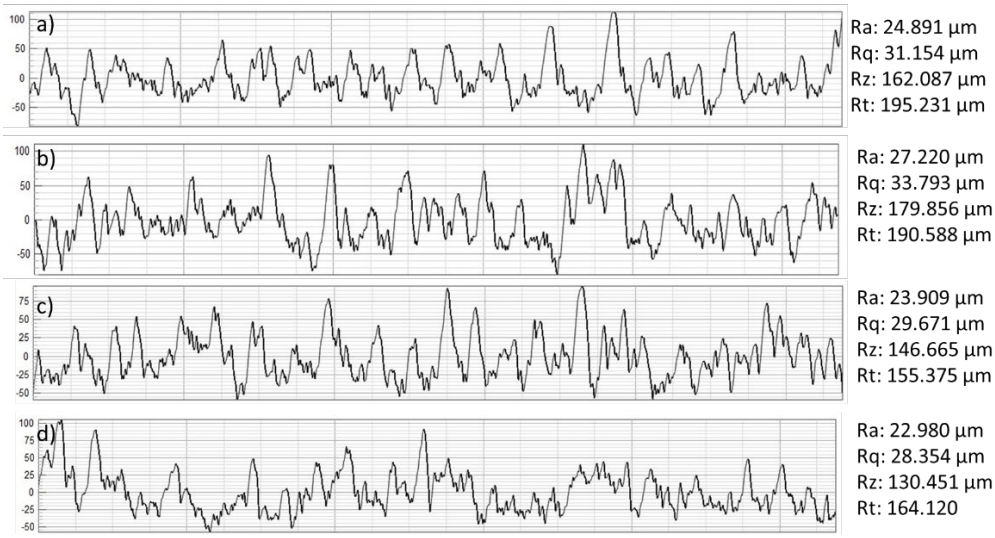

Figure 4. Surface Roughness parameters of FeCrAl samples.

3.4. Evaluation of X-Ray Diffraction

We used X-ray diffraction (XRD) analysis to determine the phase composition and structural characteristics of the coatings. The XRD patterns showed that a multiphase structure composed of metallic, intermetallic, and oxide phases. These phases originate from the combined effects of melting, oxidation, diffusion, and rapid solidification during the arc-spraying process. Below, we present the results of the XRD spectrum of each sample.

3.4.1. Sample 1

The XRD spectrum of Sample 1 (Figure 5) showed broad and intense peaks between 10° and 90° (2θ), which reflect a multiphase crystalline structure. These peaks corresponded to metallic aluminum (Al), chromium suboxide ($CrO_{0.87}$), magnetite (Fe_3O_4), and wustite [FeO (non-stoichiometric)]. We can also observe additional peaks which are associated with chromferide (FeCr) solid solutions and spinel-phase chromite ($Fe_2Cr_2O_4$). These additional peaks indicate that solid-state diffusion of Fe into Cr occurs during cooling in an oxidizing atmosphere.

The presence of both magnetite and wustite is particularly significant. Wustite forms under low oxygen partial pressure at high temperatures, and magnetite forms in more oxidizing conditions.

 doi:10.20944/preprints202602.0084.v1

Their coexistence indicates spatially non-uniform oxidation and rapid quenching (possibly due to temperature gradients and particle-substrate interaction during the deposition process). The retention of metallic aluminum and partially transformed phases supports the hypothesis of incomplete oxidation due to rapid cooling rates.

This hybrid microstructure, which consists of retained metal, spinel oxides, and sub-stoichiometric oxides, represents a well-balanced distribution of phases. This combination of phases enhances both the corrosion resistance (via stable oxides) and toughness (via retained metallic phases).

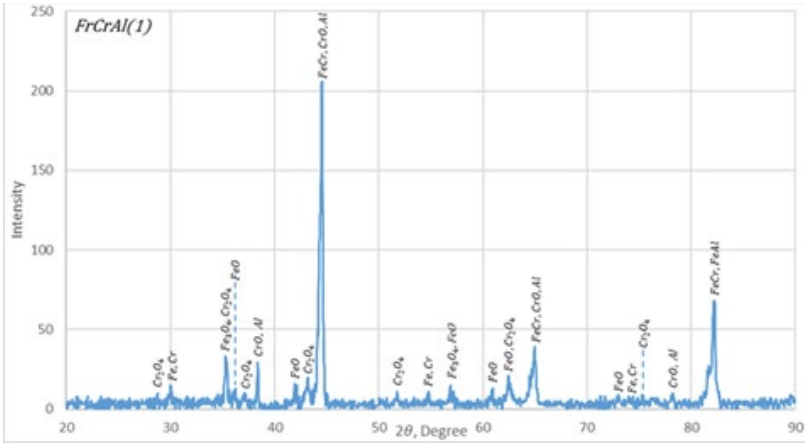

Figure 5. XRD pattern of Sample 1 showing multiphase structure with metallic phases and iron–chromium oxide compounds formed during arc spraying.

3.4.2. Sample 2

Figure 6 shows the XRD pattern of Sample 2, which contains the same major phases as Sample 1. However, we observed differences in peak intensities as changes in oxidation severity, which suggests that there is a microstructural variation between the two coatings. The key difference in Sample 2 is an increase in peak intensity for chromium suboxide ($CrO_{0.87}$) because of enhanced oxidation of Cr due to prolonged or deeper exposure to oxygen-rich plasma zones. The dominance of $CrO_{0.87}$ rather than Cr_2O_3 reflects incomplete oxidation kinetics. This might have been caused by rapid solidification or insufficient dwell time at high oxygen partial pressures.

Sample 2 also showed a higher proportion of wustite ($Fe_{0.9536}O$) relative to magnetite (Fe_3O_4). This shift indicates non-uniform thermal gradients across the sprayed surface. This phenomenon is common in arc spraying, where some zones undergo rapid cooling while others cool more slowly.

Compared to Sample 1, Sample 2 shifted toward a Cr-rich and Fe-deficient oxide matrix. This shift in microstructure indicates a subtle imbalance in oxidation dynamics, making phase formation very sensitive to small variations in process parameters. This confirms that minor changes in arc current, gas flow, or torch motion can significantly alter the phase evolution. So, strict process control is necessary during coating deposition.

 doi:10.20944/preprints202602.0084.v1

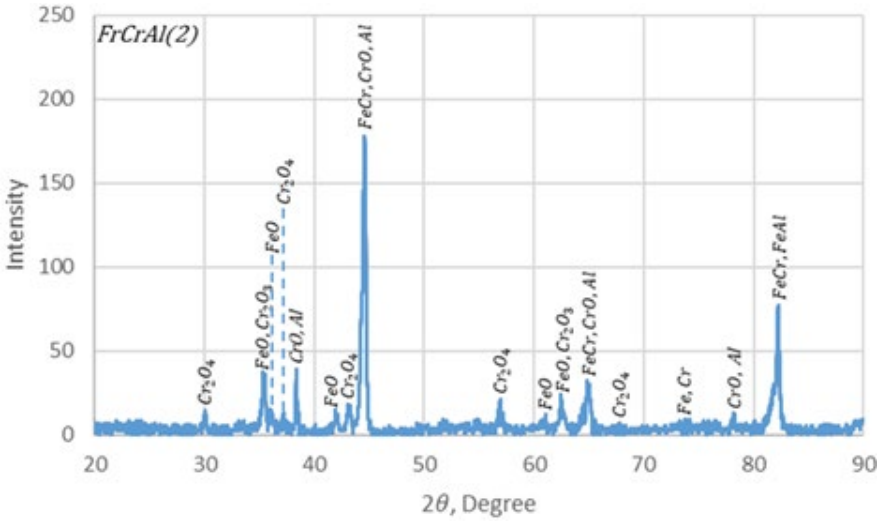

Figure 6. XRD pattern of Sample 2 showing enhanced chromium suboxide ($CrO_{0.87}$) formation and modified iron oxide phase distribution compared to Sample 1.

3.4.3. Sample 3

The XRD pattern of Sample 3 (Figure 7) showed a phase composition mostly similar to that of Samples 1 and 2. However, we can clearly detect diffraction peaks corresponding to metallic chromium (Cr). The presence of metallic Cr suggests reduced oxidation during deposition, which is mainly due to faster cooling rates or limited oxygen availability.

Such conditions might have arisen from lower effective plasma power, shorter stand-off distance, or reduced particle dwell time within the oxidizing zone. These factors can create localized low-oxygen regions that prevent complete oxidation of chromium and allow the metallic Cr to remain. This metallic chromium phase is beneficial for coatings as it can form a stable, self-healing Cr_2O_3 passive layer that improves the resistance to high-temperature oxidation.

Because of a lower level of iron oxidation, Sample 3 also exhibited weaker wustite ($Fe_{0.9536}O$) peaks compared with Samples 1 and 2. However, the continued presence of chromite spinel ($Fe_2Cr_2O_4$) confirms that diffusion-driven reactions still occurred, even under the reduced oxidation conditions. Overall, the shift toward retained Cr and lower Fe oxidation suggests a more controlled thermal history, where Cr was selectively protected while spinel phases formed, enhancing the coating's stability and durability.

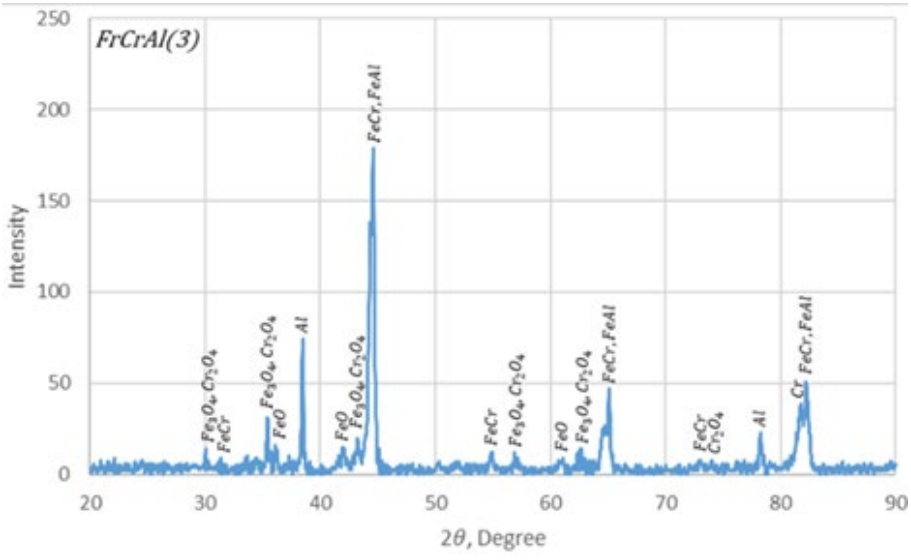

 doi:10.20944/preprints202602.0084.v1

Figure 7. XRD pattern of Sample 3 showing the presence of metallic chromium peaks and reduced iron oxide intensity, indicating lower oxidation during deposition.

3.4.4. Sample 4

Figure 8 shows the XRD pattern of Sample 4, which has the most compositionally diverse phase structure among all samples. Sample 4 uniquely exhibited diffraction peaks corresponding to Cr_2O_3 (eskolaite) and Al_2O_3 in addition to phases observed in the earlier coatings, such as metallic Al, wustite ($Fe_{0.9536}O$), chromferide (Fe,Cr), chromite ($Fe_2Cr_2O_4$), and magnetite (Fe_3O_4).

The formation of Cr_2O_3 indicates more complete chromium oxidation compared with the sub-stoichiometric $CrO_{0.87}$ observed in other samples. Eskolaite formation typically requires higher temperatures, increased oxygen availability, and slower cooling rates. Similarly, the presence of Al_2O_3 suggests significant aluminum oxidation and prolonged interaction with the plasma jet. These observations imply that Sample 4 experienced higher localized plasma temperatures and longer dwell times in oxidizing regions.

Notably, metallic chromium was detected alongside Cr_2O_3, indicating non-uniform oxidation kinetics. Some regions likely retained metallic Cr due to rapid solidification or localized shielding, while others underwent full oxidation. Such spatial variations are commonly associated with arc instability or uneven plasma flow during deposition.

The combination of Cr_2O_3 and Al_2O_3 oxides is highly advantageous for the mechanical and thermal performance of coatings. These oxides form dense and chemically stable layers that enhance wear, corrosion, and high-temperature oxidation resistance. Their presence is especially beneficial for applications involving steam-rich or aggressive environments, where protective oxide scales are essential for long-term durability.

The above XRD analysis results demonstrate that even small variations in spraying parameters can significantly influence phase formation and oxidation behavior. This sensitivity provides opportunities to produce FeCrAl coatings for specific service conditions through controlled adjustment of deposition parameters.

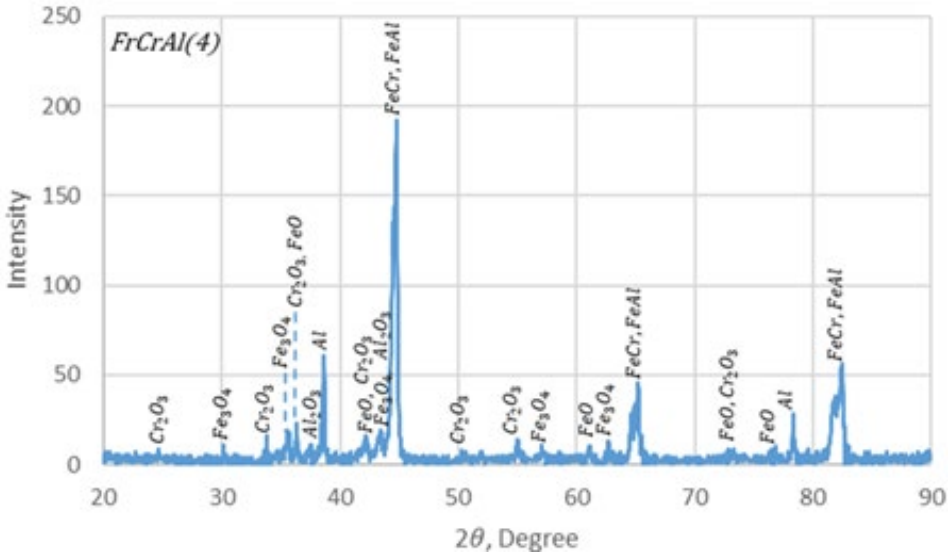

Figure 8. XRD pattern of Sample 4 showing the formation of stable oxide phases (Cr_2O_3 and Al_2O_3) together with metallic and spinel phases in the thickest coating.

3.5. Tribological Performance

As mentioned before, the tribological behavior of the FeCrAl coatings was evaluated using a TRB3 tribometer (v8.1.10) under dry sliding conditions. All samples were tested using identical parameters, including a normal load of 4.00 N, a sliding speed of 6.00 cm/s, and a wear track radius

 doi:10.20944/preprints202602.0084.v1

of 3.00 mm. Keeping these parameters constant allowed direct comparison of frictional behavior by minimizing the influence of external variables. The evolution of the coefficient of friction (CoF) as a function of sliding distance is shown in Figure 9.

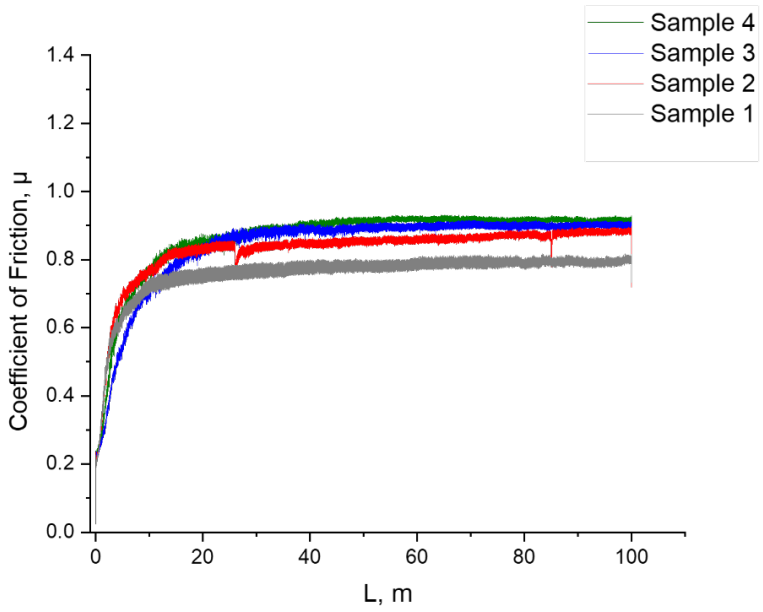

Figure 9. Coefficient of friction (CoF) evolution during dry sliding pin-on-disk tests conducted at 4 N load, 6 cm/s sliding speed, and 3 mm wear radius.

From the figure, we can notice that Sample 1 (tested at an ambient temperature of 25.18 °C and a relative humidity of 31.75%) has the most stable frictional response among all samples. The CoF stabilized below 0.85 with minimal fluctuation throughout the test. This steady behavior indicates uniform contact conditions, low debris formation, and stable interaction between the coating and the surface. The comparatively smooth surface morphology (as indicated by the surface roughness parameters in Section 3.3) and lower oxide phase content (obtained from XRD analysis in Section 3.4.1) contributed to reduced third-body effects and limited oxidation-wear interactions during sliding. Such stable friction behavior is desirable for applications requiring predictable wear performance.

Sample 2 (tested under slightly cooler and drier conditions at 21.12 °C temperature and 22.97% relative humidity) showed higher friction levels compared to Sample 1. The CoF varied between 0.043 and 0.889, with a mean value of 0.829 and an SD of 0.093. This increase in friction can be due to the higher surface roughness (Section 3.3) and oxide content, particularly chromium suboxide ($CrO_{0.87}$) (identified by XRD analysis from Section 3.4.2). High CoF promotes stronger mechanical interlocking and higher interfacial shear resistance, which increases friction during sliding.

Sample 3 showed the largest fluctuation in frictional behavior, with CoF values ranging from 0.156 to 0.910, having a mean value of 0.841 and SD = 0.127. The higher variability in CoF indicates unstable wear conditions during sliding. This behavior is likely caused by non-uniform surface oxidation and more localized surface damage due to heterogeneous oxide distribution as indicated by the XRD pattern (Section 3.4.3).

Sample 4 showed the highest mean CoF (ranging from 0.145 to 0.929) among all samples, with a mean value of 0.864 and SD = 0.115. The increased friction is consistent with the presence of hard and brittle oxide phases such as Cr_2O_3 and Al_2O_3 (as identified by XRD analysis in Section 3.4.4). These oxides can act as abrasive third-body particles during sliding, which increases surface roughness and frictional resistance.

 doi:10.20944/preprints202602.0084.v1

Overall, the tribological results demonstrate that frictional behavior is mainly governed by a combined effect of surface roughness and thickness-induced oxide phase kinetics. Although all coatings exhibited CoF values within an acceptable range (<0.93), variations in oxide content and surface roughness led to distinct tribological responses. Our study findings emphasize that we need to maintain consistent spraying conditions so that thickness-dependent oxidation effects can be controlled precisely.

4. Conclusions

In this study, we investigated the relationship between coating thickness, surface roughness, and mechanical and tribological performance of arc-sprayed FeCrAl coatings. We found that hardness remained nearly constant across all samples, which indicates that hardness is mainly controlled by the alloy composition and spray solidification behavior rather than coating geometry.

However, surface roughness and friction behavior have been strongly influenced by deposition thickness. Thicker coatings generally showed smoother surfaces due to improved splat bonding, while small variations in spraying conditions led to higher roughness and increased friction. These results show that tribological performance depends on both surface roughness and phase distribution.

The XRD patterns of samples confirmed that changes in thermal environment and oxygen availability during spraying affected the phase and oxide formation. We observed that coatings containing higher amounts of Cr_2O_3 and Al_2O_3 showed higher CoF. Overall, our results demonstrate the importance of controlling coating thickness by keeping the same arc-spraying conditions to ensure consistent surface quality and stable tribological performance.

Author Contributions: "Conceptualization, B.R. and A.K.; methodology, N.M. and S. A.; software, N.M.; validation, U.I., N.M. and E.A.; formal analysis, U.I.; investigation, U.I.; resources, B.R.; data curation, E.A.; writing—original draft preparation, S.A.; writing—review and editing, S.A. and U.I; visualization, S.A.; supervision, U.I.; project administration, A.K.; funding acquisition, A.K. All authors have read and agreed to the published version of the manuscript.".

Funding: This research has been funded by the Committee of Science of the Ministry of Science and Higher Education of the Republic of Kazakhstan. (Grant No. BR24992862).

Institutional Review Board Statement: Not applicable.

Informed Consent Statement: Not applicable.

Data Availability Statement: Data are contained within the article.

Acknowledgments:

Conflicts of Interest: The authors declare no conflicts of interest.

References

1. Babu, N.; Balasubramaniam, R.; Ghosh, A. High-temperature oxidation of Fe_3Al-based iron aluminides in oxygen. *Corros. Sci.* **2001**, 43, 2239–2254.
2. Yuan, J.; Wang, W.; Zhu, S.; Wang, F. Comparison between the oxidation of iron in oxygen and in steam at 650–750 °C. *Corros. Sci.* **2013**, 75, 309–317.
3. Agüero, A.; Baráibar, I.; Gutiérrez, M.; Tuurna, S.; Toivonen, A.; Penttilä, S.; Auerkari, P. Steam Oxidation of Aluminide-Coated and Uncoated TP347HFG Stainless Steel under Atmospheric and Ultra-Supercritical Steam Conditions at 700 °C. *Coatings* **2020**, 10, 839.
4. Castro, R.M.; Cavaler, L.C.C.; Marques, F.M.; Bristot, V.M.; Rocha, A.S. Comparative of the tribological performance of hydraulic cylinders coated by the process of thermal spray HVOF and hard chrome plating. *Tribol. Ind.* **2014**, 36, 79–89.

 doi:10.20944/preprints202602.0084.v1

5. Rakhadilov, B.; Bayatanova, L.; Kengesbekov, A.; Magazov, N.; Toleukhanova, Z.; Yeskermessov, D. Study of the influence of air plasma spraying parameters on the structure, corrosion resistance, and tribological characteristics of Fe–Al–Cr intermetallic coatings. *Coatings* **2025**, 15, 790.
6. Li, N.; Chen, L.-Y.; Chai, L.; Xuan, H.-N.; Wang, Z.; Zhang, L.; Dubovyy, O.; Zhang, J.; Lu, S. A novel plasma-sprayed Cr/FeCrAl dual-layer coating on Zr alloy for potential high-temperature applications. *J. Mater. Res. Technol*. **2024**, 30, 5569–5581.
7. Bellippady, M.; Björklund, S.; Li, X.-H.; Frykholm, R.; Kjellman, B.; Joshi, S.; Markocsan, N. Performance of atmospheric plasma-sprayed thermal barrier coatings on additively manufactured superalloy substrates. *Coatings* **2024**, 14, 626.
8. Boronenkov, V.; Korobov, Y. *Fundamentals of Arc Spraying: Physical and Chemical Regularities*; Springer: Berlin/Heidelberg, Germany, **2016**.
9. Lee, J.; Kwon, H.; Kim, Y.G.; Lee, C. Tribological and microstructural properties of carbon steel coatings fabricated by wire arc spray. *Metals Mater. Int*. **2020**, 26, 650–659.
10. Liu, G.; Rożniatowski, K.; Kurzydłowski, K.J. Quantitative characteristics of FeCrAl films deposited by arc and high-velocity arc spraying. *Mater. Charact*. **2001**, 46, 99–104.
11. Cheng, C.Q.; Zhao, J.; Cao, T.S.; Fu, Q.Q.; Lei, M.K. Facile chromaticity approach for the inspection of passive films on austenitic stainless steel. *Corros. Sci.* **2013**, 70, 235–242.
12. Liu, X.; Shao, Y.; Zhang, Y.; Meng, G.; Zhang, T.; Wang, F. Using high-temperature mechanochemistry treatment to modify iron oxide and improve the corrosion performance of epoxy coating—Part I: High-temperature ball milling treatment. *Corros. Sci*. **2015**, 90, 451–462.
13. Ndumia, J.N.; Kang, M.; Lin, J.; Liu, J.; Li, H. Influence of Heat Treatment on the Microstructure and Wear Properties of Arc-Sprayed FeCrAl/Al Coating. *Coatings* **2022**, 12, 374.
14. Ndumia, J.N.; Zhu, J.; Gbenontin, B.V.; Kang, M.; Liu, X.; Nyambura, S. M. Effect of Heat Treatment on the Microstructure and Corrosion Behavior of Arc-Sprayed FeCrAl/Al Coating. *J. Mater. Eng. Perform*. **2023**, 32, 1489–1497.
15. Liu, L.; Yang, Z.G.; Zhang, C.; Ueda, M.; Kawamura, K.; Maruyama, T. Effect of water vapour on the oxidation of Fe–13Cr–5Ni martensitic alloy at 973 K. *Corros. Sci*. **2012**, 60, 90–97.
16. Sarikaya, M. Effect of some parameters on microstructure and hardness of wire arc sprayed iron-based coatings. *Surf. Coat. Technol.* **2005**, 190, 388–393.
17. Ataiwi, A. Effect of some processing parameters on arc sprayed coating. *Eng. Technol. J*. **2008**, 26, 1554–1566.
18. Majewski, D.; Hejwowski, T.; Łukasik, D. Influence of microstructure of arc sprayed coatings on wear resistance. *Adv. Sci. Technol. Res. J*. **2018**, 12, 285–292.
19. Kim, I.-H.; Jung, Y.-I.; Kim, H.-G.; Jang, J.-I. Oxidation-resistant FeCrAl coating on Zr-alloy tubes using 3D printing direct energy deposition. *Surf. Coat. Technol*. **2021**, 411, 126915.
20. Luo, J.H.; Shi, N.; Xing, Y.Z.; Jiang, C.P.; Chen, Y.N. Effect of arc power on the wear and high-temperature oxidation resistance of plasma-sprayed Fe-based amorphous coatings. *High Temp. Mater. Process*. **2019**, 38, 639–646.
21. Li, B.; Fan, L.; Bai, J.; He, J.; Su, J.; Wang, S.; Deng, C.; Liu, S.; Zhang, Z. Study on porosity of thermal-sprayed commercially pure aluminum coating. *Materials* **2023**, 16, 6612.
22. Li, N.; Chen, L.-Y.; Wang, Z.-X.; Xuan, H.-N.; Chai, L.-J.; Yang, H.-L.; Dubovyy, O.; Lu, S. Enhancement of hardness and high-temperature oxidation resistance of Cr/FeCrAl dual-layer plasma-sprayed coating on Zr substrate by post-processing. *J. Mater. Res. Technol*. **2025**, 36, 500–512.
23. Brundle, C.R.; Chuang, T.J.; Wandelt, K. Core and valence level photoemission studies of iron oxide surfaces and the oxidation of iron. *Surf. Sci.* **1977**, 68, 459–468.
24. Yamashita, T.; Hayes, P. Analysis of XPS spectra of Fe^{2+} and Fe^{3+} ions in oxide materials. *Appl. Surf. Sci*. **2008**, 254, 2441–2449.
25. Hu, H.; Zhou, Z.; Li, M.; Zhang, L.; Wang, M.; Li, S.; Ge, C. Study of the corrosion behavior of an 18Cr oxide dispersion strengthened steel in supercritical water. *Corros. Sci.* **2012**, 65, 209–213.
26. Gao, Y.; Chambers, S.A. Heteroepitaxial growth of α-Fe_2O_3, γ-Fe_2O_3 and Fe_3O_4 thin films by oxygen-plasma-assisted molecular beam epitaxy. *J. Cryst. Growth* **1997**, 174, 446–454.

27. Kengesbekov, A. Influence of plasma arc current and gas flow on the structural and tribological properties of TiN coatings obtained by plasma spraying. *Coatings* **2024**, 14, 1404.
28. Pogrebnjak, A.D.; Bagdasaryan, A.A.; Beresnev, V.M.; Nyemchenko, U.S.; Ivashchenko, V.I.; Kravchenko, Y.O.; Shaimardanov, Z.K.; Plotnikov, S.V.; Maksakova, O. Effects of Cr and Si additions and deposition conditions on the structure and properties of (Zr–Ti–Nb) N coatings. *Ceram. Int*. **2017**, 43, 771–782.
29. Mamaeva, A.; Kenzhegulov, A.; Panichkin, A.; Abdulvaliyev, R.; Fischer, D.; Bakhytuly, N.; Toiynbaeva, N. Influence of current duty cycle and voltage of micro-arc oxidation on the microstructure and composition of calcium phosphate coating. *Coatings* **2024**, 14, 766.
30. Yermakhanova, A.M.; Kenzhegulov, A.K.; Meiirbekov, M.N.; Baiserikov, B.M. Comparative study of dielectric characteristics and radio transparency of composite materials. *J. Elastomers Plast*. **2024**, 56, 843–857.
31. Rakhadilov, B.; Magazov, N.; Kakimzhanov, D.; Apsezhanova, A.; Molbossynov, Y.; Kengesbekov, A. Influence of Spraying Process Parameters on the Characteristics of Steel Coatings Produced by Arc Spraying Method. *Coatings* **2024**, 14, 1145.